A three-step reconstruction method for fluorescence molecular tomography based on compressive sensing

Yansong Zhu[a], Abhinav K. Jha[b], Jakob K. Dreyer[c], Hanh N. D. Le[a], Jin U. Kang[a], Per E. Roland[c], Dean F. Wong[b], and Arman Rahmim[a,b]

[a]Department of Electrical and Computer Engineering, Johns Hopkins University, Baltimore, USA
[b]Department of Radiology, Johns Hopkins University, Baltimore, USA
[c]Department of Neuroscience and Pharmacology, University of Copenhagen, Copenhagen, Denmark

ABSTRACT

Fluorescence molecular tomography (FMT) is a promising tool for real time in vivo quantification of neurotransmission (NT) as we pursue in our BRAIN initiative effort. However, the acquired image data are noisy and the reconstruction problem is ill-posed. Further, while spatial sparsity of the NT effects could be exploited, traditional compressive-sensing methods cannot be directly applied as the system matrix in FMT is highly coherent. To overcome these issues, we propose and assess a three-step reconstruction method. First, truncated singular value decomposition is applied on the data to reduce matrix coherence. The resultant image data are input to a homotopy-based reconstruction strategy that exploits sparsity via ℓ_1 regularization. The reconstructed image is then input to a maximum-likelihood expectation maximization (MLEM) algorithm that retains the sparseness of the input estimate and improves upon the quantitation by accurate Poisson noise modeling. The proposed reconstruction method was evaluated in a three-dimensional simulated setup with fluorescent sources in a cuboidal scattering medium with optical properties simulating human brain cortex (reduced scattering coefficient: 9.2 cm^{-1}, absorption coefficient: 0.1 cm^{-1}) and tomographic measurements made using pixelated detectors. In different experiments, fluorescent sources of varying size and intensity were simulated. The proposed reconstruction method provided accurate estimates of the fluorescent source intensity, with a 20% lower root mean square error on average compared to the pure-homotopy method for all considered source intensities and sizes. Further, compared with conventional ℓ_2 regularized algorithm, overall, the proposed method reconstructed substantially more accurate fluorescence distribution. The proposed method shows considerable promise and will be tested using more realistic simulations and experimental setups.

Keywords: FMT, reconstruction, compressive sensing, noise modeling

1. INTRODUCTION

Fluorescence molecular tomography (FMT) is an emerging technique for 3D visualization and quantification of biomarkers *in vivo*,[1] and has received much research interest for its applications such as small animal imaging and tumor study.[2,3] In our BRAIN Initiative project, we are attempting to quantify the neurotransmitter effects *in vivo* via voltage sensitive dyes that emit radiation and optical wavelengths.[4] For this purpose we are designing a FMT system. The objective is to use the detector measurements made by this system to reconstruct the distribution of the voltage sensitive dyes within the biological tissue. However, this reconstruction problem is highly ill posed due to the limited number of measurements and the high amount of scattering of photons in the biological tissue. Consequently, a unique solution for the fluorescence distribution in the source is often hard to find. To overcome the ill-posed nature of the problem, several different regularization studies have been proposed. Conventionally used strategies, such as the Tikhonov regularization[5] and Laplacian regularization,[6]

Further author information: (Send correspondence to Abhinav K. Jha)
Abhinav K. Jha: E-mail: ajha4@jhmi.edu

Optical Tomography and Spectroscopy of Tissue XII, edited by Bruce J. Tromberg, Arjun G. Yodh, Eva Marie Sevick-Muraca, Robert R. Alfano, Proc. of SPIE Vol. 10059, 1005911 · © 2017 SPIE
CCC code: 1605-7422/17/$18 · doi: 10.1117/12.2252664

attempts to minimize the ℓ_2 norm. The drawback of such regularization strategy is that it tends to generate over-smooth edges,[7] which makes the resulting image look blurry.

In many applications, the fluorescence signal can be treated as sparse over the entire field of view. Based on this information, the ℓ_1 regularized least-square problem can be formulated for the pursuit of a sparse result. Such kind of ℓ_1 regularized problems have received substantial interest in the field of compressive sensing (CS) and different methods have been proposed to solve this problem.[8–10] These methods usually require restricted isometry property (RIP) to be satisfied, which in turn means that the columns of measurement matrix should be almost incoherent. However, due to the scattering within the biological tissue, the measurement matrix is hightly coherent, so existing CS methods are not directly applicable. A truncated singular value decomposition (TSVD) method has been suggested before applying the sparse-recovery techniques to reduce the coherence of measurement matrix.[11] We also note that images acquired by FMT systems are corrupted by Poisson noise. Although several sparse reconstruction methods have been reported for the FMT problem,[11,12] these methods do not model Poisson noise, which makes the reconstruction results less reliable. To compensate for this noise, we incorporate a noise-compensation strategy.

In the following part, we propose a three-step reconstruction method for FMT problem, which involves conversion of the measurement matrix, sparse reconstruction and noise compensation. This work is part of our BRAIN initiative effort. In addition, in this BRAIN initiative effort, we are also investigating analytical methods to model light propagation through tissue.[13]

2. METHOD

2.1 Theory

2.1.1 Forward Model

Consider a FMT system consisting of a fluorescent source within a scattering medium. The fluorescent source is excited by a laser. The radiation emitted by this source is detected by a detector. Let $x(\mathbf{r})$ denotes the fluorescence distribution at position $\mathbf{r}$, where $\mathbf{r}$ is a three-dimensional vector, and let $g_{\text{ex}}(\mathbf{r}, \mathbf{r_s})$ and $g_{\text{em}}(\mathbf{r_d}, \mathbf{r})$ denote the excitation and emission Green's function that describe photon propagation from laser source at position $\mathbf{r}_s$ to the fluorescent source at position $\mathbf{r}$, and from fluorescent source at position $\mathbf{r}$ to the detector at position $\mathbf{r_d}$, respectively. Then the forward model of FMT problem can be described as:

$$\Phi(\mathbf{r_d}, \mathbf{r_s}) = \int_\Omega g_{\text{em}}(\mathbf{r_d}, \mathbf{r}) x(\mathbf{r}) g_{\text{ex}}(\mathbf{r}, \mathbf{r_s}) d^3 r, \tag{1}$$

where Ω denotes the object support for the fluorescence distribution.

This equation can be discretized in the spatial domain along the object coordinates and the detector coordinates using the voxel basis. Let Φ_{mn} denotes the fluorescent signal generated by the n^{th} laser source put at the corresponding voxel at $\mathbf{r_s}$ and detected by the m^{th} detector put at the corresponding voxel at $\mathbf{r_d}$. x_i denotes the fluorescence distribution at the i^{th} voxel. g_{ni}^{em}, g_{mi}^{ex} denote Green's function describing excitation light from the n^{th} laser source to fluorescent source in the i^{th} voxel, and emission light from fluorescent source in the i^{th} voxel to the m^{th} detector. For object space containing N voxels, equation (1) after discretization becomes:

$$\Phi_{mn} = \sum_{i=1}^{N} g_{ni}^{\text{ex}} g_{im}^{\text{em}} x_i. \tag{2}$$

If we use one laser source and M detectors to build the system, the matrix formation of the above equation is

$$\mathbf{\Phi} = \mathbf{G}\mathbf{X}, \tag{3}$$

where the measurement vector is

$$\mathbf{\Phi} = \begin{bmatrix} \Phi_{11} \\ \Phi_{21} \\ \vdots \\ \Phi_{M1} \end{bmatrix},$$

the measurement matrix is

$$\mathbf{G} = \begin{bmatrix} g_{11}^{\text{em}} g_{11}^{\text{ex}} & g_{12}^{\text{em}} g_{21}^{\text{ex}} & \cdots & g_{1N}^{\text{em}} g_{N1}^{\text{ex}} \\ g_{21}^{\text{em}} g_{11}^{\text{ex}} & g_{22}^{\text{em}} g_{21}^{\text{ex}} & \cdots & g_{2N}^{\text{em}} g_{N1}^{\text{ex}} \\ \vdots & \vdots & \cdots & \vdots \\ g_{M1}^{\text{em}} g_{11}^{\text{ex}} & g_{M2}^{\text{em}} g_{21}^{\text{ex}} & \cdots & g_{MN}^{\text{em}} g_{N1}^{\text{ex}} \end{bmatrix},$$

and the vector of fluorescence distribution for reconstruction is

$$\mathbf{X} = \begin{bmatrix} x_1 \\ x_2 \\ \vdots \\ x_N \end{bmatrix}.$$

Due to scattering, matrix $\mathbf{G}$ is highly coherent. However, using an SVD based approach, this coherence can be reduced, as described below.

2.1.2 Coherence Reduction

Using singular value decomposition, the matrix $\mathbf{G}$ can be writen as

$$\mathbf{G} = \mathbf{U}\mathbf{\Sigma}\mathbf{V}^T, \tag{4}$$

where $\mathbf{U}$, $\mathbf{V}$ are unitary matrices, and $\mathbf{\Sigma}$ is a diagonal matrix with singular values as its diagonal. T denotes transpose of a matrix. For $M \times N$ matrix $\mathbf{G}$, if $M < N$ and the rank of $\mathbf{G}$ is M, the singular matrix $\mathbf{\Sigma}$ can be written as: $\mathbf{\Sigma} = \begin{bmatrix} \mathbf{\Sigma}_t & \mathbf{0} \end{bmatrix}$, where $\mathbf{\Sigma}_t$ is an $M \times M$ diagonal matrix with non-zero singular value as the diagonal elements. This yields:

$$\mathbf{G}_{M\times M} = \mathbf{U}\mathbf{\Sigma}_t\mathbf{V}^T.$$

Inserting this expression into equation (4) yields

$$\mathbf{\Phi} = \mathbf{U}\mathbf{\Sigma}_t\mathbf{V}^T\mathbf{X}. \tag{5}$$

Applying the operator $\mathbf{\Sigma}_t^{-1}\mathbf{U}^{-1}$ on both sides of the equation and using the fact that $\mathbf{U}$ is unitary so that $\mathbf{U}^{-1} = \mathbf{U}^T$ yields

$$\mathbf{\Sigma}_t^{-1}\mathbf{U}^T\Phi = \mathbf{V}^T\mathbf{X} \tag{6}$$

Next, we define $\mathbf{Y} = \mathbf{\Sigma}_t^{-1}\mathbf{U}^T\mathbf{\Phi}$, and $\mathbf{A} = \mathbf{V}^T$. Then we get a new matrix equation written as

$$\mathbf{Y} = \mathbf{A}\mathbf{X}. \tag{7}$$

This new measurement matrix $\mathbf{A}$ has relatively lower coherence compared to the original matrix $\mathbf{G}$.[11] Thus, it is possible to implement a CS-based reconstruction method on the measurement matrix A. The CS-based algorithm that exploits the sparsity is discussed in the following section.

2.1.3 Sparse Reconstruction

The reconstruction problem can be described with the following ℓ_1 regularized least-square minimization problem:

$$\min_X F(X) = \frac{1}{2}\|\mathbf{A}\mathbf{X} - \mathbf{Y}\|_2^2 + \lambda\|\mathbf{X}\|_1, \tag{8}$$

where $F(X)$ is objective function, and λ is regularization parameter.

To solve this minimization problem, we use a homotopy-based method.[12,14] First, subdifferential of the objective function $F(X)$ is given by:

$$\partial F(X) = -\mathbf{A}^T(\mathbf{Y} - \mathbf{A}\mathbf{X}) + \lambda\partial\|\mathbf{X}\|_1, \tag{9}$$

where subdifferential $\partial\|\mathbf{X}\|_1$ can be written as

$$\partial\|\mathbf{X}\|_1 = \left\{ u \in R^n \middle| \begin{array}{ll} u_i = \mathrm{sgn}(X_i), & X_i \neq 0 \\ u_i \in [-1,1], & X_i = 0 \end{array} \right\}. \tag{10}$$

Define $\mathbf{c} = \mathbf{A}^T(\mathbf{Y} - \mathbf{AX})$, which denotes vector of residual correlations. To minimize objective function $F(X)$, we set $\partial F(X) = 0$. This is equivalent to the following two conditions:

$$c_j = \lambda \mathrm{sgn}(x_j), \text{ for } x_j \neq 0, \tag{11}$$

and

$$|c_j| \leq \lambda, \text{ for } x_j = 0. \tag{12}$$

The algorithm starts with initial guess $\mathbf{X} = \mathbf{0}$, and chooses $\lambda = \|\mathbf{c}\|_\infty = \max\{\mathbf{c}\}$. We define an active set I that contains indices j that satisfies condition $|c_j| = \lambda$, i.e., $I = \{j : |c_j| = \lambda\}$. For each iteration, only those elements of $\mathbf{X}$ are updated whose indices are contained in I. Using $\mathbf{A}_I$ to denote matrix formed with columns of $\mathbf{A}$ in active set I, for l^{th} iteration, the vector of update direction $\mathbf{d}_I^{(l)}$ is obtained by solving

$$\mathbf{A}_I^T \mathbf{A}_I \mathbf{d}_I^{(l)} = \mathrm{sgn}(\mathbf{c}_I^{(l)}). \tag{13}$$

$\mathbf{d}^{(l)}$ is set to zero for coordinates that are not in I. Vector $\mathbf{X}$ is updated with

$$\mathbf{X}^{(l)} = \mathbf{X}^{(l-1)} + \gamma^{(l)} \mathbf{d}^{(l)}, \tag{14}$$

where $\gamma^{(l)}$ is the step size to next breakpoint along homotopy path. In each interation, the step size is updated based on whether equation (11) or equation (12) is followed. First, when equation (12) is violated, which means a nonactive element of $\mathbf{c^{(l)}}$ increase in magnitude beyond λ, this leads to the expression

$$\gamma_+^{(l)} = \min_{i \in I^c}{}^{+} \{ \frac{\lambda - c_i^{(l)}}{1 - \mathbf{a}_i^T \mathbf{v}^{(l)}}, \frac{\lambda + c_i^{(l)}}{1 + \mathbf{a}_i^T \mathbf{v}^{(l)}} \}, \tag{15}$$

where $\min_{i \in I^c}^{+}$ indicates the minimum is taken only for positive arguments that do not belong to set I, $\mathbf{v}^{(l)} = \mathbf{A}_I^T \mathbf{d}_I^{(l)}$ and $\mathbf{a}_i$ is the i^{th} column in matrix $\mathbf{A}$. Second, when equation (11) is violated, which means an active coordinate crosses zero. In this case, the following expression is obtained:

$$\gamma_-^{(l)} = \min_{i \in I}{}^{+} \{ -x_i^{(l)} / d_i^{(l)} \}. \tag{16}$$

Finally, $\gamma^{(l)}$ is determined as

$$\gamma^{(l)} = \min\{\gamma_+^{(l)}, \gamma_-^{(l)}\}. \tag{17}$$

For every iteration, the active set is updated by either adding i_+ to set I when $\gamma^{(l)} = \gamma_+^{(l)}$, or removing i_- from I when $\gamma^{(l)} = \gamma_-^{(l)}$. The algorithm terminates when $\|\mathbf{c}^{(l)}\|_\infty = 0$ for noise-free case.

While this procedure attempts to exploit sparsity, the measured data is always contaminated by noise and $\|\mathbf{c}^{(l)}\|_\infty$ cannot reach zero. Thus, we set a threshold α for $\|\mathbf{c}^{(l)}\|_\infty$. When, $\|\mathbf{c}^{(l)}\|_\infty < \alpha$, the algorithm stops iterating. Next, we will describe how to statistically model the noise in the reconstruction process.

2.1.4 Noise Modeling

To reduce the influence of Possion noise, the result from homotopy method is then sent to MLEM algorithm as the initializing image. the MLEM iterative algorithm can be described with the following formula:[15]

$$\hat{x}_n^{k+1} = \hat{x}_n^k \frac{1}{s_n} \sum_{m=1}^{M} \frac{y_m}{(\mathbf{H}\hat{\mathbf{x}}^k)_m} H_{mn}, \tag{18}$$

where s_n is n^{th} component of point sensitive vector and is written as

$$s_n = \sum_{m=1}^{M} H_{mn}. \tag{19}$$

The initial guess $\hat{\mathbf{x}}^1$ is formulated with non-zero component of reconstruction result $\mathbf{X}$ in equation (8). Matrix $\mathbf{H}$ consists of corresponding rows in matrix $\mathbf{A}$.

2.2 Experiment Procedure

To validate the proposed method, a 3D numerical cubic phantom was built, as shown in figure 1. The phantom was discretized into $20 \times 20 \times 20$ voxels, with the size of 1 mm^3 for each voxel. The optical properties of the phantom were set as: absorption coefficient: 0.1 cm^{-1}, reduced scattering coefficient: 9.2 cm^{-1}. These parameters replicate the optical properties of human brain cortex for our application of quantification of NT effects. A fluorescence source in the shape of a cuboid with the size of 4 mm $\times$ 4 mm $\times$ 8 mm was at the center of the phantom. Measurements were taken at five surface of the phantom (top surface and four side surfaces). One laser source was put at the center of the top surface. The size of measurement matrix is 884×8000. Poisson noise was added to the measurement vector $\mathbf{\Phi}$. In this experiment, the Green's function in the forward model was generated using the MC method namely Monte Carlo eXtreme (MCX).[16]

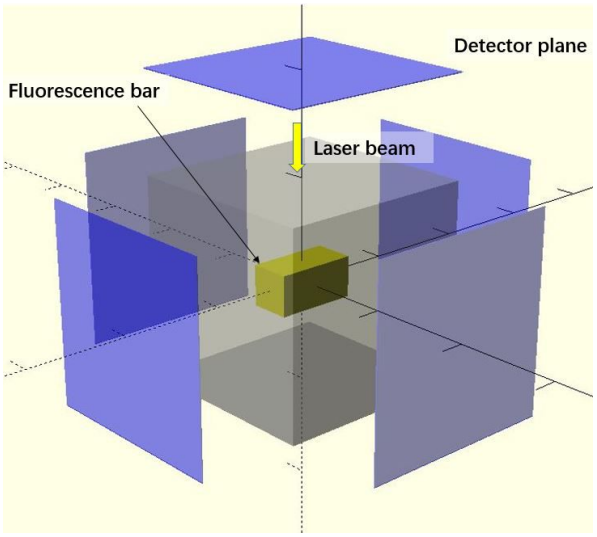

Figure 1: Setup of numerical cube phantom experiment

The proposed method was compared with conventionally used ℓ_2 norm method. We choose Tikhonov regularization method as comparison in this experiment. The minimization problem with this regularization is given by:

$$\min_X F(X) = \frac{1}{2}\|\mathbf{AX} - \mathbf{Y}\|_2^2 + \frac{\lambda}{2}\|\mathbf{X}\|_2^2, \tag{20}$$

where λ is regularization parameter.

To objectively evaluate the performance of this technique on the task of estimating fluorescence activity within the cuboidal region of interest, we calculate root mean square error (RMSE) and bias. Given a set of reconstructed data $\hat{\mathbf{X}}$ with N elements, if we use $\mathbf{X}$ to denote the true value, RMSE is given by:

$$RMSE = \sqrt{\frac{1}{N}\sum_{i=1}^{N}\left(\hat{X}_i - X_i\right)^2}. \tag{21}$$

The bias is calculated using the formula:

$$Bias = \frac{1}{N}\sum_{i=1}^{N}\left(\hat{X}_i - X_i\right). \tag{22}$$

3. RESULTS

First, we show reconstruction results of the proposed method and commonly used ℓ_2 norm method. In this experiment, the regularization parameter of Tikhonov regularization was set as $\lambda = 1 \times 10^{-3}$. On the other hand, the stopping creteria in the proposed method was chosen as $\alpha = 1 \times 10^{-3}$ so that the iteration stoped when $\|\mathbf{c}^{(l)}\|_\infty < \alpha$. The reconstruction results of these two methods are shown in figure 2.

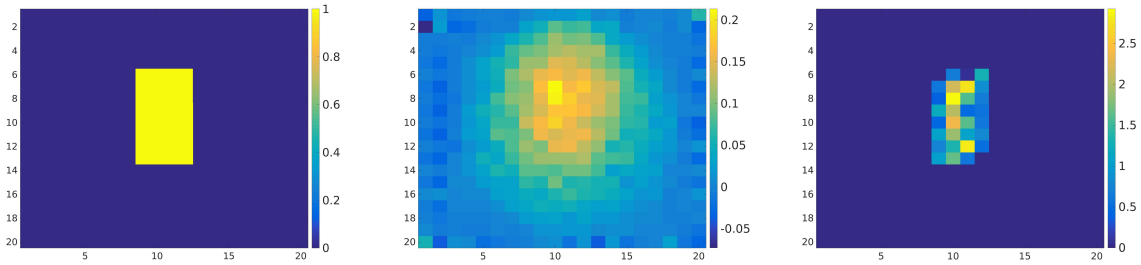

(a) (b) (c)

Figure 2: Reconstruction results for numerical cube phantom experiment. a: slice of true fluorescent targets. b: slice of reconstruction result with Tikhonov regularization method. c: slice of reconstruction result with the proposed method

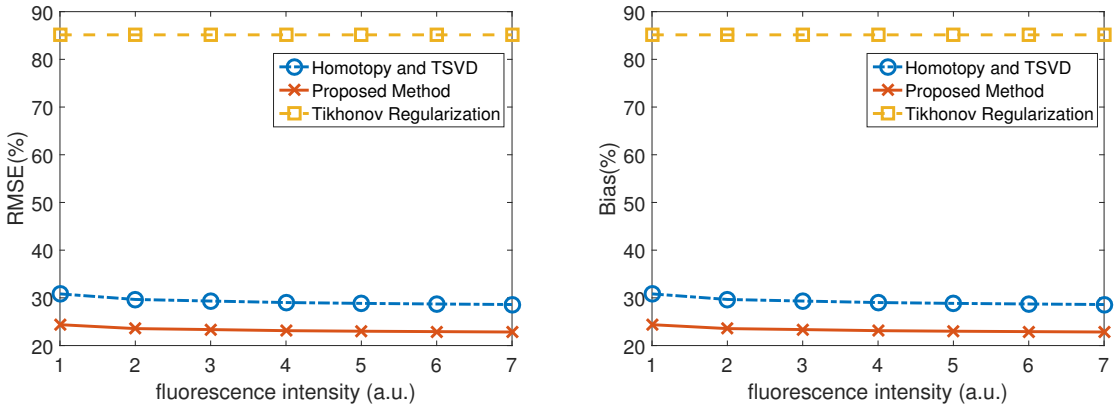

(a) (b)

Figure 3: Comparison among Tikhonov regularization method, TSVD and homotopy method, and proposed method with MLEM step. a: comparison of RMSE for different fluorescence signal intensity. b: comparison of bias for different fluorescence signal intensity.

Next, we studied the effect of MLEM algorithm for noise reduction. Since direct homotopy reconstruction did not generate meaningful results, we chose homotopy reconstruction after TSVD for comparison instead, together with ℓ_2 norm regularization method, and the proposed method. Figrue 3 shows the RMSE and bias of reconstruction results for these three methods. The fluorescence signal intensity varied during the experiments,

and experiments were repeated 10 times for each intensity. The average RMSE for Tikhonov regularization method is 85.14%, for TSVD and homotopy method is 29.29%, and for proposed method with MLEM step is 24.06%.

4. DISCUSSION AND CONCLUSION

From figure 2, the proposed method gave a better performance. It provided a clear background, sharp edges and relative accurate fluorescence intensity in the reconstruction image. On the other hand, the method using Tikhonov regularizer generated a blurry reconstruction image. This was expected since, as menthioned in the Introduction, this regularizer can introduce oversmoothing. From figure 3a, we notice that the proposed method, with or without MLEM step, gave much lower RMSE compared to the Tikhonov regularization method. Further, the MLEM step reduced the RMSE about 5% on average compared with method without the MLEM step. Figure 3b shows that the reduction of RMSE mainly came from the reduction of bias. These result demonstrate the necessity of modeling Poisson noise for accurate reconstruction.

In conclusion, we presented a three-step method for FMT reconstruction problem. The method involves 1)TSVD, 2)homotopy method for solving ℓ_1 norm minimization problem and 3)MLEM iterations for reducing Poisson noise. Numerical phantom experimentation was conducted to validate the feasibility of the method. Our ongoing work involves digital animal phantom, *in-vivo* animal experiment for further validation. Further, based on some of our previous work,[17–19] we are investigating the idea of objective evaluation to optimize fluorescence imaging systems.

ACKNOWLEDGMENTS

This work was supported by the NIH BRAIN Initiative Award R24 MH106083.

REFERENCES

[1] Chen, J. and Intes, X., "Comparison of Monte Carlo methods for fluorescence molecular tomography—computational efficiency," *Medical Physics* **38**, 5788 (2011).

[2] Ntziachristos, V., Ripoll, J., Wang, L. H. V., and Weissleder, R., "Looking and listening to light: the evolution of whole-body photonic imaging," **23**, 313–320– (2005).

[3] Montet, X., Figueiredo, J., Alencar, H., Ntziachristos, V., Mahmood, U., and Weissleder, R., "Tomographic fluorescence imaging of tumor vascular volume in mice," *Radiology* **242**(3), 751–758 (2007).

[4] Jha, A. K., Zhu, Y., Dreyer, J., Kang, J., Gjedde, A., Wong, D., and Rahmim, A., "Incorporating boundary conditions in the integral form of the radiative transfer equation for transcranial imaging," *Biomedical Optics 2016* , JW3A.47, Optical Society of America (2016).

[5] Serdaroglu, A., Yazici, B., and Ntziachristos, V., "Fluorescence molecular tomography based on a priori information," *Biomedical Topical Meeting* , SH46, Optical Society of America (2006).

[6] Davis, S. C., Dehghani, H., Wang, J., Jiang, S., Pogue, B. W., and Paulsen, K. D., "Image-guided diffuse optical fluorescence tomography implemented with laplacian-type regularization," *Optics express* **15**(7), 4066–4082 (2007).

[7] Behrooz, A., Zhou, H.-M., Eftekhar, A. A., and Adibi, A., "Total variation regularization for 3d reconstruction in fluorescence tomography: experimental phantom studies," *Appl. Opt.* **51**, 8216–8227 (Dec 2012).

[8] Tropp, J. A. and Gilbert, A. C., "Signal recovery from random measurements via orthogonal matching pursuit," *IEEE Trans. Inf. Theor.* **53**, 4655–4666 (Dec. 2007).

[9] Friedman, J., Hastie, T., and Tibshirani, R., "Regularization paths for generalized linear models via coordinate descent," *Journal of statistical software* **33**(1), 1 (2010).

[10] Efron, B., Hastie, T., Johnstone, I., Tibshirani, R., et al., "Least angle regression," *The Annals of statistics* **32**(2), 407–499 (2004).

[11] Shi, J., Cao, X., Liu, F., Zhang, B., Luo, J., and Bai, J., "Greedy reconstruction algorithm for fluorescence molecular tomography by means of truncated singular value decomposition conversion," *J. Opt. Soc. Am. A* **30**, 437–447 (Mar 2013).

[12] Xue, Z., Ma, X., Zhang, Q., Wu, P., Yang, X., and Tian, J., "Adaptive regularized method based on homotopy for sparse fluorescence tomography," *Appl. Opt.* **52**, 2374–2384 (Apr 2013).

[13] Jha, A. K., Zhu, Y., Wong, D. F., and Rahmim, A., "A radiative transfer equation-based image-reconstruction method incorporating boundary conditions for diffuse optical imaging," *SPIE Medical Imaging 2017* , accepted, SPIE (2017).

[14] Donoho, D. L. and Tsaig, Y., "Fast solution of-norm minimization problems when the solution may be sparse," *IEEE Transactions on Information Theory* **54**(11), 4789–4812 (2008).

[15] Barrett, H. H. and Myers, K. J., [*Foundations of Image Science*], Wiley (2003).

[16] Fang, Q. and Boas, D. A., "Monte carlo simulation of photon migration in 3d turbid media accelerated by graphics processing units," *Opt. Express* **17**, 20178–20190 (Oct 2009).

[17] Jha, A. K., Kupinski, M. A., Masumura, T., Clarkson, E., Maslov, A. V., and Barrett, H. H., "Simulating photon-transport in uniform media using the radiative transport equation: a study using the neumann-series approach," *J. Opt. Soc. Am. A* **29**, 1741–1757 (Aug 2012).

[18] Jha, A. K., Kupinski, M. A., Barrett, H. H., Clarkson, E., and Hartman, J. H., "Three-dimensional neumann-series approach to model light transport in nonuniform media," *JOSA A* **29**(9), 1885–1899 (2012).

[19] Jha, A. K., Clarkson, E., and Kupinski, M. A., "An ideal-observer framework to investigate signal detectability in diffuse optical imaging," *Biomedical optics express* **4**(10), 2107–2123 (2013).